KeAi

CHINESE ROOTS
GLOBAL IMPACT

Contents lists available at ScienceDirect

Petroleum Science

journal homepage: www.keaipublishing.com/en/journals/petroleum-science



Original Paper

Molecular simulation of the solubility of hydrocarbon oligomers in supercritical CO₂ for direct viscosification



Ying Sun a, Bin Wang b,c, Haizhu Wang b,c, Boxin Ding a,b,c,*

- ^a School of Advanced Materials, Peking University Shenzhen Graduate School, Shenzhen, 518055, Guangdong, China
- ^b College of Petroleum Engineering, China University of Petroleum (Beijing), Beijing, 102249, China
- ^c State Key Laboratory of Petroleum Resources and Engineering, China University of Petroleum (Beijing), Beijing, 102249, China

ARTICLE INFO

Article history: Received 15 October 2024 Received in revised form 24 February 2025 Accepted 14 May 2025 Available online 15 May 2025

Edited by Min Li

Keywords: CO₂ viscosification Hydrocarbon oligomers Molecular simulation Dissolution mechanism Methyl groups

ABSTRACT

Direct viscosification of CO₂ offers promising alternative for mobility control and reduction in residual brine saturation, thus to improve the CO₂ trapping in saline aquifers. Hydrocarbon oligomers, recognized for their exceptional properties, are considered as one of the most promising viscosifiers in displacement of brine-saturated porous media. However, the molecular-level mechanisms governing the solubility and viscosification of hydrocarbon oligomers in scCO2 remain poorly understood. In this study, we employ coarse-grained molecular models to advance our understanding in the effects of molecular structure of hydrocarbon oligomers on their solubility in scCO₂. The coarse-grained models of five hydrocarbon oligomers with different numbers of methyl-branch (n-C32, P1D-2, P1D-3, P1D-6 and squalane) are established to investigate their effects on solubilization in scCO₂. We demonstrate that the number of methyl groups has a monotonic correlation with the solubility of hydrocarbon oligomers when the molecular weights of oligomers are comparable. The radial distribution function reveals n-C32, P1D and squalane are uniformly dispersed with separation distances of approximately 1.0-2.0 nm. The interaction energy between hydrocarbon oligomers and CO₂ shows that the number of methylbranch in hydrocarbon oligomers can directly influence their solubility in scCO2. Molecular simulation results demonstrate that the interaction distances between the methyl-branch and CO2 are smaller than those of other molecular fragments. There are approximately 20% more CO₂ molecules interacting with methyl-branch than with other parts. This work sets the stage for our future molecular dynamics study in viscosification by hydrocarbon oligomers with different branching length and interfacial phenomena in multiphase systems.

© 2025 The Authors. Publishing services by Elsevier B.V. on behalf of KeAi Communications Co. Ltd. This is an open access article under the CC BY-NC-ND license (http://creativecommons.org/licenses/by-nc-nd/4.0/).

1. Introduction

Carbon capture, utilization, and storage (CCUS) technology is an indispensable and important means to achieve carbon neutrality (Middleton et al., 2015; Hou et al., 2017). Sites selected for CO₂ storage include saline aquifers, depleted oil and gas reservoirs, coal seams, etc. Among them, saline aquifers have been found in most continent, demonstrating enormous carbon storage capacity (Firoozabadi and Myint, 2010). The mechanisms of CO₂ storage in saline aquifers include structural and stratigraphic trapping, residual trapping, solubility trapping, and mineral trapping.

* Corresponding author.

E-mail address: boxin.ding@cup.edu.cn (B. Ding).

Due to low CO_2 viscosity at the subsurface often found in supercritical conditions, the injected CO_2 may spread quickly at the formation top below the caprock. This results in a high probability of CO_2 leakage (Al-Abri et al., 2012; Shokrollahi et al., 2013). Several techniques have been developed in the past decades to improve the mobility ratio of CO_2 to in-situ resident fluids, such as water-alternating-gas (WAG) injection (Christensen et al., 2001), carbonated water injection (Riazi et al. 2011a, 2011b), CO_2 foam (Rossen et al. 2022), and direct viscosification (Heller et al., 1985). The WAG method can effectively reduce the preferential flow of water and lower the risk of waterflooding. However, this technique involves frequent injection operations and requires precise control over the injection ratios and timing of CO_2 and water (Christensen et al., 2001). The carbonated water injection can significantly reduce the oil-water interfacial tension and improve oil mobility.

However, the acidic components in carbonate water may cause corrosion to pipelines and equipment (Riazi et al. 2011a, 2011b). The CO₂ foam barriers in the reservoir can promote selective driving of the oil layer (Ding et al. 2020, Ding et al., 2021). However, the surfactants used in the foam preparation process tend to adsorb onto the rock surfaces, which may lead to pore blockage and disrupt flow pathways. Additionally, CO₂ foam usually requires high pumping pressure, causing an injection concern (Rossen et al. 2022). Compared to these three methods, there is no requirement of water injection for the direct viscosification of CO₂. CO₂ viscosification may also be helpful for improved oil recovery (Song et al., 2019) and geothermal development (Feng et al., 2021; Feng and Firoozabadi, 2023). Takuma et al. (2024) clarify that CO₂ fracturing is superior to water fracturing in creating a more complex fracture pattern at a lower injection pressure, but it is not suitable for creating large-aperture fractures in rocks with relatively low porosity/permeability. Therefore, they propose combined CO2-water fracturing, in which CO2 creates fractures first, and then water opens/propagates the fractures. Li and Zhang (2019) propose that scCO₂ fracturing followed by viscosified CO₂ fracturing can readily create complex fracture networks and carry proppants to keep fractures open. A good fracturing performance can effectively enhance the permeability of geothermal reservoirs, which is beneficial for the heat extraction.

Traditional CO₂ viscosifiers generally include fluorinated polymers, siloxane polymers, and hydrocarbon polymers (Li et al., 2024). Each type of these viscosifiers has its advantages and disadvantages. Fluorinated polymers exhibit strong interactions with CO₂ due to their low cohesive energy density and strong CO₂ affinity, resulting in excellent solubility (Hoefling et al. 1991). Fluorinated compounds are currently the most effective viscosifiers reported. These polymers, characterized by carbon-fluorine bonds, can increase CO₂ viscosity without co-solvents (Shen et al., 2003). Despite their effectiveness in enhancing CO₂ viscosity, fluoropolymers typically require dissolution pressures exceeding 30 MPa. The adsorption of these molecules onto the rock surface is strong (Zaberi et al. 2020). In addition, the fluorinated polymers are generally expensive for synthesis and the difficult degradation poses environmental concerns (Gandomkar et al., 2023). These factors limit their widespread application. Siloxane polymers, consisting of Si-O-Si main chain structures, are modified by introducing functional groups on their side chains or chain ends to improve CO₂ solubility and hinder CO₂ molecular mobility, thereby exhibiting significant CO₂ viscosification properties (Li et al., 2018). While more CO₂-philic than hydrocarbon polymers, siloxane polymers do not achieve effective CO2 viscosification without the addition of substantial amounts of co-solvents. Their strong adsorption onto the rock surface makes siloxane polymers unsuitable for field applications, considering the costs and co-solvent usage (Li et al., 2024). Based on the drawbacks of other polymers, researchers have turned their attention to hydrocarbon polymers. Composed primarily of carbon and hydrogen atoms, hydrocarbon polymers are simple, readily available, and environmentally friendly (Goicochea and Firoozabadi, 2019; Kar and Firoozabadi, 2022; Ricky et al., 2023). Afra et al. (2023) conducted brine displacement experiments with scCO₂ in sandstone. The experimental results showed that a concentration of 1.5 wt% viscosifier increased the viscosity of scCO₂ by 4.8 times at a pressure of 3,500 psi and a temperature of 194 °F. The viscosified CO₂ had a reduced mobility and CO₂ breakthrough was delayed by 200%–300%. To accurately acquire the in-situ saturation of the scCO2 in the sandstone core, Ding et al. (2024b) utilize the X-ray CT imaging techniques to investigate neat and viscosified CO2 in displacement of brine-saturated porous media. They demonstrate the effectiveness of the oligomer of 1-decene with 17 repeat units (P1D-17, average MW = 2,900 g/mol) in improvements in brine production and breakthrough delay at a low concentration of 0.6 wt%. Additionally, they design and synthesize a new molecule; it is an oligomer with branches of 1-dodecene with 6 repeat units and 1hexadecene also with 6 repeat units (average MW = 2.500 g/mol). The new oligomer is reported to increase residual trapping of CO₂ in saline aquifers by about 35 %. More recently, Ding et al. (2024a) examined the sweep efficiency and residual brine saturation in the layered cores by effective viscosification with two engineered molecules by X-ray CT imaging. In comparison to the neat CO₂ injection, the synergistic effect of the mobility control and increases in interfacial elasticity by injection of vis-CO₂ results in delay in breakthrough by a factor of 2 and about 95% higher brine production. The design and selection of the viscosifier molecules are mainly based on the following criteria: desired solubility in CO₂; effective CO₂ viscosification; very low adsorption onto the rock surfaces; very low solubility in water; high partitioning in CO₂ in the presence of an oil phase; mild effect from brine and temperature; and environmental friendliness (Kar and Firoozabadi, 2022). However, CO₂ viscosification by hydrocarbon polymers remain controversial, primarily focused on the following two points. Firstly, the research on the CO2 viscosification of the currently most representative hydrocarbon oligomer, poly-1decene (P1D), has led to different conclusions among various scholars. The early work by Heller et al. (1985) and recent works by Lemaire et al. (2021) and Shah et al. (2024) show that P1D with six repeat units has a marginal effect on viscosification of scCO₂. However, the works by Kar and Firoozabadi (2022), Al-Hinai et al. (2018) and Zhang et al. (2011) show that P1D may achieve a more than 40% viscosity increase. Ding et al. (2024b) have discussed and listed the potential causes on the differences in the experimental measurements by the above-stated literature. Secondly, the viscosification mechanism of hydrocarbon polymers is still highly controversial. Some scholars believe that hydrocarbon polymers thicken CO₂ primarily through chain entanglement, while others suggest that the polymers are singly-dispersed in CO₂ (Hong et al., 2008). Additionally, Kobayashi and Firoozabadi (2023) found that the solubility of poly(1-decene) with nine repeat units is higher in CO₂ than poly(1-dodecene) with six repeat units. It indicates that the polymer branching also plays an important role in CO₂ viscosification. Therefore, further research is urgently needed to elucidate the viscosification mechanism of hydrocarbon polymers in CO_2 .

The goal of this work is to investigate the structural dependency of hydrocarbon oligomer solubility in CO2 and elucidate the intrinsic mechanism of solubilization at the molecular level, advancing our understanding of dissolution mechanisms of viscosifier molecules in scCO₂. Here, we screen hydrocarbon oligomers with various methyl-branched structures and calculate their solubility in scCO₂ through molecular dynamics simulation (MD). This study explores the relationship between the number of methyl groups in hydrocarbon oligomers and their solubility in scCO₂. Additionally, we investigate the distribution morphology of hydrocarbon oligomers in scCO₂ and further examine the interaction strength between different parts of the oligomer molecules and CO₂. This study reveals the mechanisms of solubilization and viscosification of hydrocarbon oligomers in scCO₂. Our research provides theoretical support for the application of CO2 viscosification in CO₂ geological sequestration, CO₂-enhanced oil and gas recovery, geothermal development, and CO₂ fracturing.

2. Methods

2.1. Molecular dynamics simulation

The MD is performed using the GROMACS (Van der Spoel et al., 2005; Schmid et al., 2011) 2022.5 package with a time step of 1 fs. Simulations are performed in the NPT ensemble with the temperature and pressure controlled using the V-rescale thermostat and the Parrinello-Rahman barostat (Parrinello and Rahman, 1981), respectively. Referring to the work of Kobayashi and Firoozabadi (2023), a cutoff length of 1.4 nm is applied for nonbonded interactions. Particle mesh Ewald summation (Darden et al., 1993) is utilized to calculate long-range electrostatic interactions with a short-range cutoff of 1.4 nm. Considering the simulation time and system size, we employed the coarse-grained models in this study (shown in Fig. 1).

The coarse-grained model of n-C32 (molecular weight, MW = 450 g/mol) is from An et al. (2018). This model could predict the experimental properties with different timesteps, system sizes, and temperatures with reasonable accuracy (An et al., 2018). To reflect the chain structure of the squalane, a united atom force field is used which has been proven to effectively reflect the interfacial phenomena of squalane (MW = 422 g/mol) (Martin and Siepmann, 1999). The coarse-grained molecular parameters representing P1D-2 (P1D with two repeat units, MW = 283 g/mol), P1D-3 (P1D with three repeat units, MW = 423 g/mol) and P1D-6 (P1D with six repeat units, MW = 843 g/mol) come from Kobayashi and Firoozabadi (2023). A single-site model of CO₂ (MW = 44 g/mol) is proposed by Higashi et al. (1998). The model reproduces pressure dependency of the density of CO₂ and is used

to investigate the phase behavior of binary systems (Senapati et al., 2002).

2.2. The solubility calculation method

We used the direct coexistence method (DCM) to calculate the solubility of hydrocarbon oligomers in scCO₂. In this method, we placed the solute and solvent in the same simulation box and directly measured the solubility by allowing the system to reach equilibrium through simulation (Manzanilla-Granados et al., 2015; Espinosa et al., 2016). Firstly, the direct coexistence interfacial system is established (shown in Fig. 2). We ensured that an excess of oligomer molecules is added to each oligomer-CO2 interfacial system. For different systems, we kept the number of added molecules (600 oligomer and 50,000 CO2 molecules) and the initial size of the simulation box (10 nm \times 10 nm \times 40 nm) consistent. To prepare initial configurations, the individual equilibration simulations of pure CO₂ and pure oligomers systems under the conditions required for solubility calculations are needed. Secondly, we employed the NPT ensemble, using the Nosé-Hoover thermostat (Nose, 1984; Hoover, 1985) and the Parrinello-Rahman barostat (Parrinello and Rahman, 1981) to maintain stable temperature and pressure in the system. The simulations are run for a sufficient duration to ensure that the system reached complete equilibrium. Finally, we utilized the density profile to calculate the concentrations of the solute and solvent at equilibrium, thereby obtaining accurate solubility. The illustration of the calculation method is shown in Fig. 3(a). The last 10 ns of the simulation trajectory is selected to compute partial densities across the box, and the average density variation values of the hydrocarbon

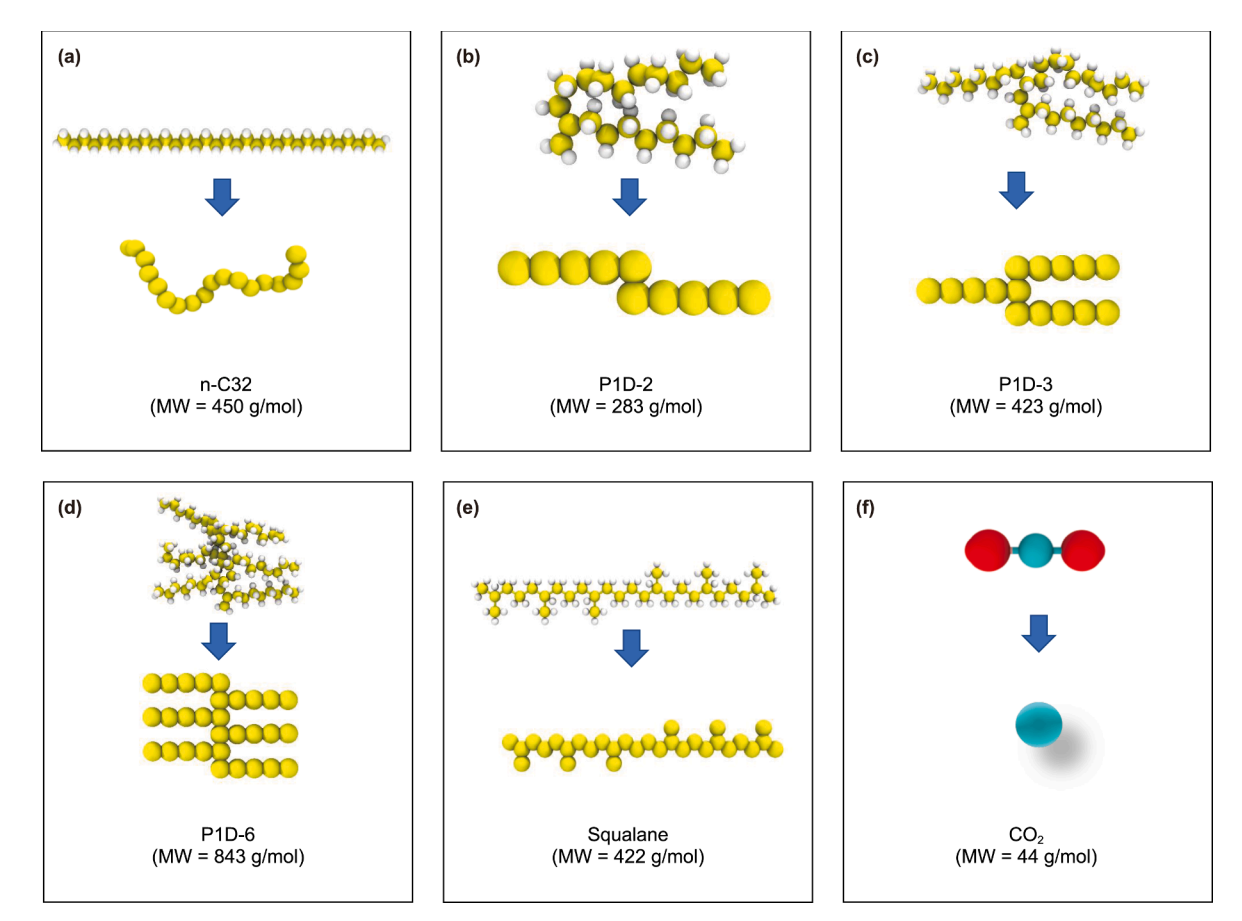


Fig. 1. The coarse-grained model of (a) n-C32, (b) P1D-2, (c) P1D-3, (d) P1D-6, (e) squalane and (f) CO₂.

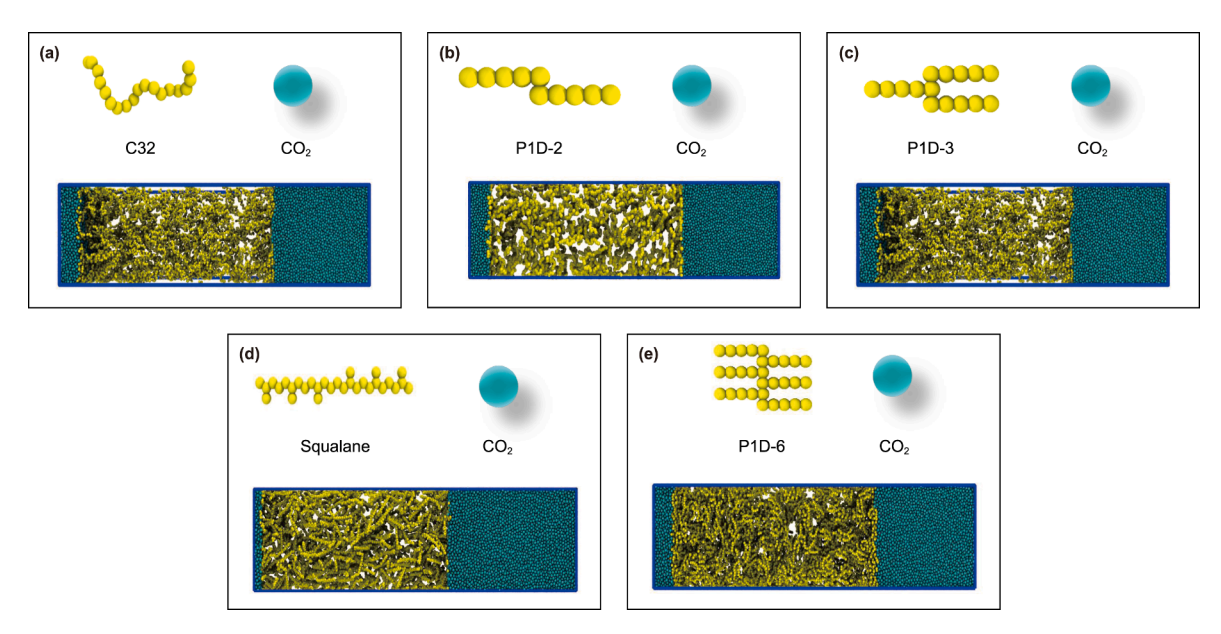


Fig. 2. The direct coexistence interfacial system of (a) n-C32, (b) P1D-2, (c) P1D-3, (d) squalane, (e) P1D-6 and CO2.

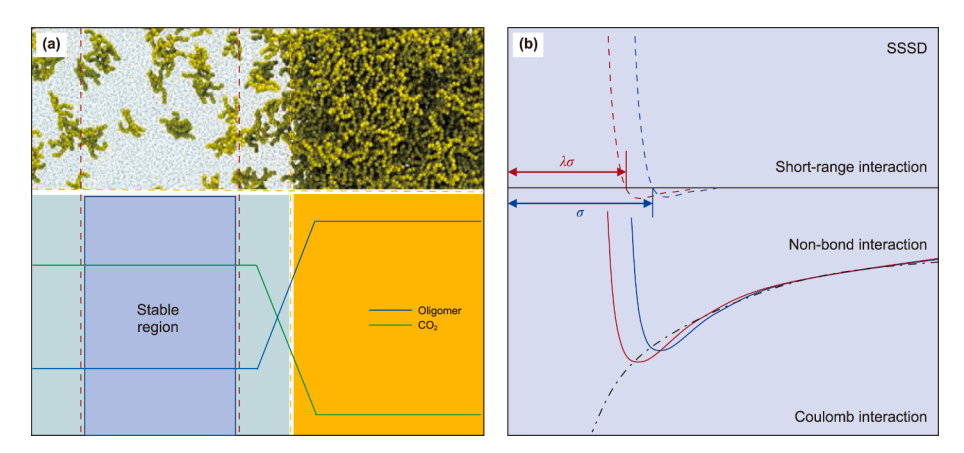


Fig. 3. Illustration of simulation methods: (a) the direct coexistence simulation method, in which solute solubility is determined in the stable region; (b) the scaled solute-solvent distance (SSSD) method (Sun et al., 2023).

oligomer and CO_2 along the Z-axis direction of the simulation box are extracted. Based on the density variation data, select the dissolution stable region and calculate the average density of the oligomer (D_0) and the CO_2 density (D_{CO_2}) in the stable region. Then, calculate the solubility (S_{0-CO_2}) using the formula: $S_{0-CO_2} = D_0 / (D_0 + D_{CO_2})$.

2.3. The scaled solute-solvent distance method

To better match the simulated predictions of oligomer solubility with experimental values, we employ a simple and effective method, scaled solute-solvent distance (SSSD), which specifically optimizes the force field parameters (Sun et al., 2023). In the SSSD method, the parameters in the short-range potentials that relate to the distance between solute and solvent (e.g., σ in the LJ potential and ρ in the Buckingham potential) are multiplied by a scaling factor λ , $\sigma_{scaled} = \lambda \sigma$ (Fig. 3(b)). The scaling factors are adjusted until the predicted solubility by the modified force field matches the experimental measurements. We choose to scale the parameter related to the solute-solvent distances for two reasons. First, adjusting the cross-term parameters (i.e., the parameters to

describe the solute-solvent interactions) does not affect the solute-solute and solvent-solvent interactions, thus avoiding reparameterization. Second, adjusting the distance-related parameters can change the potential energies more effectively compared to adjusting the energy-related parameters.

2.4. The radial distribution function (RDF)

The RDF, also known as $g_{AB}(r)$, is a measure used in statistical mechanics and MD to describe how particle density varies as a function of distance from a reference particle. It provides detailed insights into the spatial distribution and structure of particles in a system, particularly in liquids (Brehm and Kirchner, 2011). The definition of g(r) is the ratio of the average particle density between r and $r + \Delta r$ to the overall average particle density, as shown in Eq. (1) (Hu et al., 2015; Sun et al., 2018).

$$g_{\mathrm{AB}}(r) = \frac{1}{\rho_{\mathrm{AB}} \cdot 4\pi r^2 \cdot \Delta r} \frac{\sum_{j=1}^{N_{\mathrm{AB}}} \Delta N_{\mathrm{AB}}(r \rightarrow r + \Delta r)}{N_{\mathrm{AB}}} \tag{1}$$

where $g_{AB}(r)$ is the RDF value, ρ_{AB} is the bulk density, N_{AB} is the

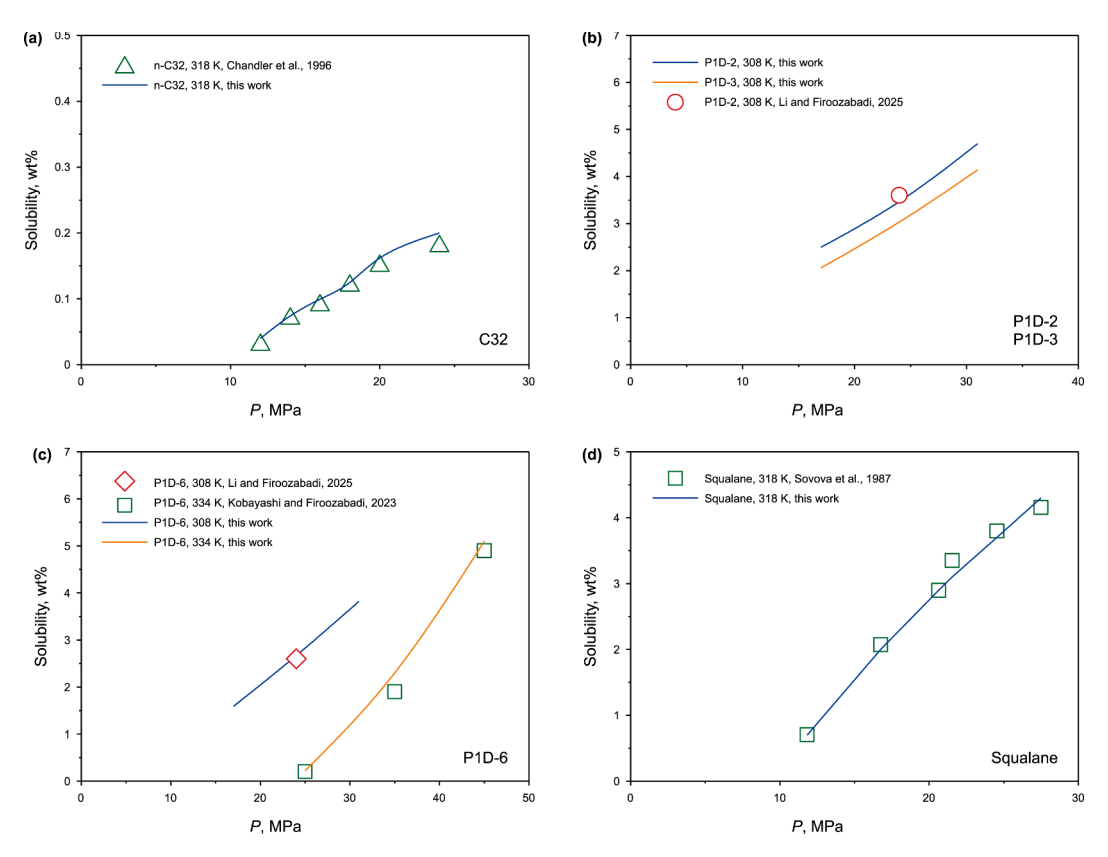


Fig. 4. Comparison of our simulation results with previous work. solubility of (a) n-C32, (b) P1D-2, P1D-3, (c) P1D-6 and (d) squalane, in scCO₂ at T = 308, 318, 334 K.

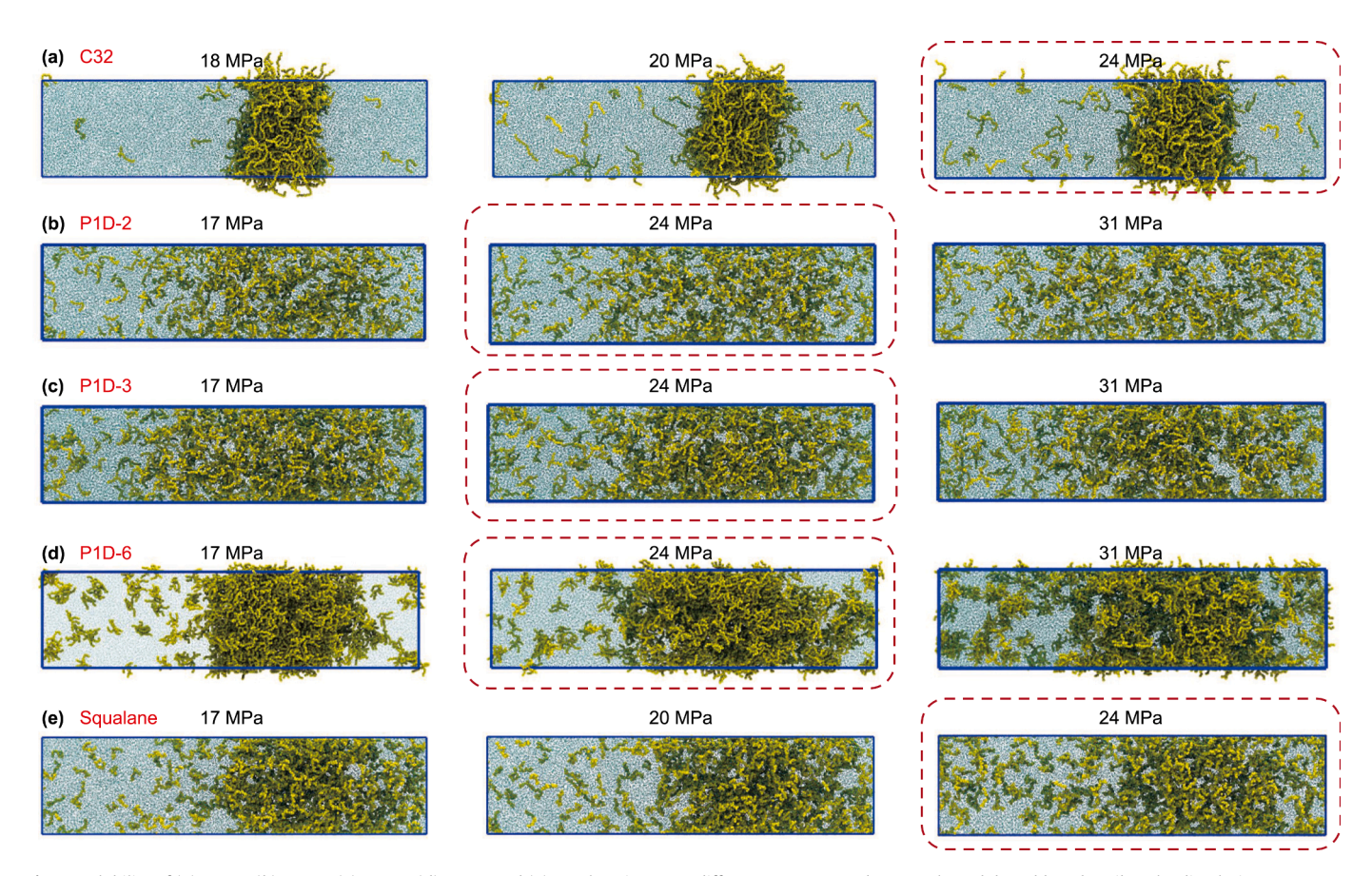


Fig. 5. Solubility of (a) n-C32, (b) P1D-2, (c) P1D-3, (d) P1D-6 and (e) squalane in CO₂ at different pressures and 308 K. The red dotted box describes the dissolution at 24 MPa.

number of particles A and B, and ΔN_{AB} means the particle number of A (or B) around B (or A) from r to $r + \Delta r$.

2.5. The interaction energy calculation method

The interaction energy can quantitatively describe the strength of the hydrocarbon oligomer- CO_2 interaction, where a larger absolute value indicates a stronger interaction between the hydrocarbon oligomer and CO_2 (Ho et al., 2010). The interaction energy could be used to predict compatibility among the components of the system. By simulating the total energy of each system under stable structures, the interaction energy between polymer chains and CO_2 can be calculated using the following expression (Hu et al., 2015):

$$E_{\text{inter}} = E_{\text{oligomer} + \text{CO}_2} - \left(E_{\text{oligomer}} + E_{\text{CO}_2}\right)$$
 (2)

where $E_{\rm inter}$ represents the interaction energy between the polymer chain and CO₂, which is equal to the negative value of the binding energy $E_{\rm binding}$. $E_{\rm oligomer+CO_2}$ is the total energy of the hydrocarbon oligomer dissolved in the CO₂ system. $E_{\rm oligomer}$ is the energy of the pure hydrocarbon oligomer system. And $E_{\rm CO_2}$ is the energy of the pure CO₂ system.

3. Results and discussion

3.1. The solubility of hydrocarbon oligomers in CO₂

Hydrocarbon oligomers are simple, readily available, and environmentally friendly, and they are currently considered to have great potential as CO₂ viscosifiers. The ability to dissolve in scCO₂ is a prerequisite for effective viscosification performance by hydrocarbon oligomers. Therefore, we calculated the solubility of n-C32 (with two methyl groups), P1D-2 (with three methyl groups), P1D-3 (with four methyl groups), P1D-6 (with seven methyl groups) and squalane (with eight methyl groups) under different pressures and temperatures. The simulation results are compared with experimental data as shown in Fig. 4.

In Fig. 4, it can be observed that the solubility values predicted by our simulation (dashed lines) closely match the experimentally measured solubility values (points). This demonstrates that our simulation method is reasonable and that the values obtained from the simulation are accurate, effectively verifying the reliability of our simulation. Furthermore, from the results, we can observe that the pressure has a significant impact on the solubility of hydrocarbon oligomers in scCO₂. The solubility of different hydrocarbon oligomers in scCO₂ increases with rising pressure, but the extent of their increase varies greatly. To illustrate more intuitively the changes in solubility of different hydrocarbon oligomers at various pressure levels, we extract the final frame image from the simulations, as shown in Fig. 5.

In Fig. 5, it is evident that the solubilities of n-C32, squalane, P1D-2, P1D-3 and P1D-6 increase significantly with rising pressure. However, the solubility of different hydrocarbon oligomers at the same pressure varies considerably. For instance, at 24 MPa, the solubility of squalane (3.8 wt%) is much higher than that of other hydrocarbon polymers, among which n-C32 has the lowest solubility, only 0.2 wt%.

We compare the solubility under various temperature and pressure conditions of n-C32 with two methyl groups, P1D-2 with three methyl groups, P1D-3 with four methyl groups, P1D-6 with seven methyl groups, and squalane with eight methyl groups. Fig. 6 shows the solubility of hydrocarbon oligomers as a function of the number of methyl groups. There is a positive correlation

between the number of methyl groups and their solubility in $scCO_2$ when the molecular weight of the hydrocarbon oligomers is comparable.

3.2. Distribution morphology of hydrocarbon oligomers

We investigate the distribution morphology of hydrocarbon oligomers in scCO₂ to elucidate the viscosification mechanism of hydrocarbon oligomers in scCO₂. We construct three cubic simuboxes that have the lation same $(20 \text{ nm} \times 20 \text{ nm} \times 20 \text{ nm})$. All the boxes contain the same number of CO₂ molecules (100,000) and different numbers of hydrocarbon oligomer molecules. We determine the number of hydrocarbon oligomer molecules to be added based on solubility calculations under various pressures. Ensuring the addition of hydrocarbon oligomer molecules, the concentration of these oligomers in the simulation boxes is slightly lower than their theoretical solubility values. To more intuitively observe the distribution morphology of different hydrocarbon oligomers in scCO₂, we extract images of the final frames of the simulation boxes for n-C32, squalane, P1D-2, P1D-3 and P1D-6 under various pressure conditions as shown in Fig. 7. In Fig. 7, we observe that the n-C32, P1D-2, P1D-3, P1D-6 and squalane molecules are present in a dispersed state within scCO₂. One may conclude that the viscosification by the hydrocarbon oligomers is not achieved through the molecular entanglement, but rather through the molecular interaction of the dispersed molecules with scCO₂.

To more accurately elucidate the distribution morphology between the oligomer and oligomer molecules, we calculate the RDF as shown in Fig. 8. In Fig. 8, all RDFs for the five types of hydrocarbon oligomer exhibit two distinct peaks. At these peaks, the density ratios of the hydrocarbon oligomers are significantly greater than 1, indicating that the densities of the hydrocarbon oligomers at these points are higher than the average density of the system. The distribution patterns of n-C32 and P1Ds (P1D-2, P1D-3 and P1D-6) are quite similar, with the first significant peak in their RDFs appearing at approximately 2.5 nm. This indicates a typical separation distance of 2.5 nm between n-C32-n-C32 and P1D-P1D molecules. In the spatial range of 0–2 nm, the RDF values of the hydrocarbon oligomers (n-C32 and P1D) are close to 0. This indicates that the probability of one hydrocarbon oligomer

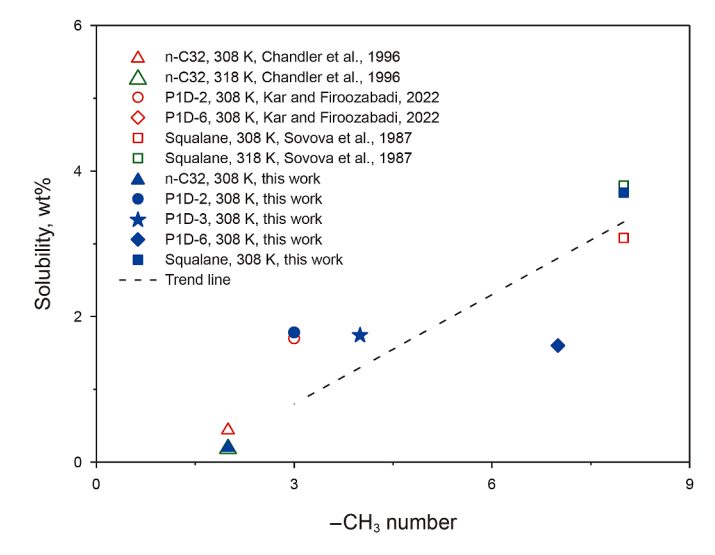


Fig. 6. Solubility of n-C32, P1D-2, P1D-3, P1D-6 and Squalane in $scCO_2$ at T=308, 318 K and P=24 MPa.

molecule appearing within a 2 nm radius of a reference hydrocarbon oligomer molecule is nearly 0. Combined with the distribution morphology of the hydrocarbon oligomers diagram as shown in Fig. 7, it demonstrates that when the hydrocarbon oligomers dissolve in scCO₂, there is approximately a 2 nm spatial distance between the molecules. The separation distance between squalane molecules is smaller than that of the other two hydrocarbon oligomers, with an average spacing of about 1.5 nm. Similar to P1Ds and n-C32, the RDF value of squalane approaches 0 at distances less than 1 nm. This indicates that although squalane has a more compact distribution morphology in scCO₂ compared to P1Ds and n-C32, there is still a 1 nm spatial distance between molecules, without any entanglement or connection. In the context of the distribution morphology of hydrocarbon oligomers in scCO₂, the RDF quantifies the spatial distances between the oligomer molecules. One may conclude that the hydrocarbon oligomers are uniformly dispersed and exhibit some preferred separation distances of approximately 1-2 nm. This demonstrates that the hydrocarbon oligomers exist in a dispersed state within scCO₂. This morphology of molecular distribution sets the stage for elucidating the mechanism how these hydrocarbon oligomers viscosify CO₂ in our future molecular simulation.

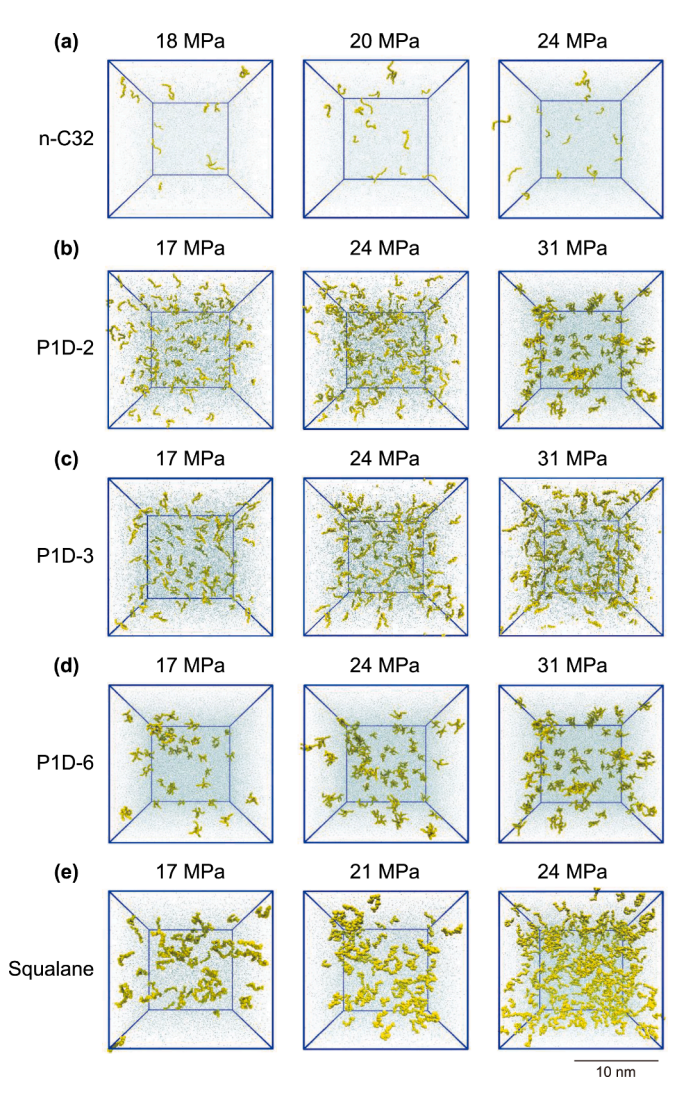


Fig. 7. Distribution morphology of (a) n-C32, (b) P1D-2, (c) P1D-3, (d) P1D-6 and (e) squalane under various pressures and temperature of 308 K.

3.3. The interactions between hydrocarbon oligomers and CO₂

In the hydrocarbon oligomer- CO_2 system, the interaction between the hydrocarbon oligomer and CO_2 serves as a critical driving force influencing the solubility of the hydrocarbon oligomer. A whole in its ground state has lower energy compared to the separated phases, which is why this system can remain in a stable state.

Therefore, we need to establish separate simulation systems for pure CO_2 and hydrocarbon oligomers, as well as a simulation system where hydrocarbon oligomers are dissolved in CO_2 , as shown in Fig. 9. We ensure that the quantity of oligomer molecules and CO_2 molecules added in different hydrocarbon oligomer systems remains consistent, only varying the types of oligomers.

The energy of $50,000 \text{ CO}_2$ molecules, the energies of eight molecules for different types of hydrocarbon oligomer (n-C32, squalane, P1D-2, P1D-3 and P1D-6), and the total energy of the system after thorough mixing of the eight hydrocarbon oligomer molecules with $50,000 \text{ CO}_2$ molecules are obtained through molecular dynamics simulations. In terms of Eq. (7), we calculate the interaction energies between different types of hydrocarbon oligomers and CO₂ at 24 MPa and 308 K, with the results presented in Table 1.

As shown in Table 1, the interaction energy of squalane with CO₂ is significantly greater than that of the other hydrocarbon oligomers. The absolute value is 6100 kJ/mol. This indicates that squalane has the highest solubility in CO2, which may be attributed to its maximum number of methyl groups. The interaction of n-C32 with CO₂ is also the lowest among the five hydrocarbon oligomers, only 4200 kJ/mol. And the absolute value of the interaction energy of P1D-3 with CO₂ is 5311 kJ/mol. Although squalane, n-C32 and P1D-3 have comparable molecular weights, squalane has 8 methyl groups which is larger than 4 methyl groups of P1D-3 and 2 methyl groups of n-C32. As a result, the interaction of squalane with CO₂ is higher than that of P1D-3 and n-C32. In addition, the absolute values of the interaction energy of P1D-2 and P1D-6 with CO₂ are 5372 kJ/mol and 5039 kJ/mol, respectively. The comparison of results indicates that the number of methyl groups in hydrocarbon oligomers can directly influence the magnitude of their interaction with CO2. And the magnitude of interaction between hydrocarbon oligomers and CO2 directly affects their solubility in scCO₂.

3.4. The impact of methyl branching on the solubility

To further investigate the impact of methyl branching on solubility, we examine the interactions between different segments of hydrocarbon oligomers and CO₂. Based on the coarse-grained modeling approach, we divide the n-C32, squalane, P1D-2, P1D-3 and P1D-6 molecules into distinct segments as shown in Fig. 10. The n-C32 molecule is divided into methyl-containing end-chain beads (C2E) and methyl-free main-chain beads (C2M). The squalane molecule is divided into methine (C1), methylene (C2), and methyl (C3) beads. The P1D molecules (P1D-2, P1D-3 and P1D-6) are divided into main-chain head beads (C2EB), main-chain beads (C2MB), mid-branch beads (C2M), and end-chain beads (C2E). To elucidate the interaction distances between different fragments of hydrocarbon polymer molecules and CO₂ molecules, we plot the RDF of different fragments with CO₂ in n-C32, squalane, and P1D molecules as shown in left column in Fig. 11.

In left column in Fig. 11, the interaction distances between the methyl-bearing fragments (C2E, C3) and CO_2 are smaller than those of other types of molecular fragments. Taking squalane as an example, the interaction distance between the methyl group (C3) and CO_2 is only 3.05 Å, while the methylene group (C2) is 3.15 Å,

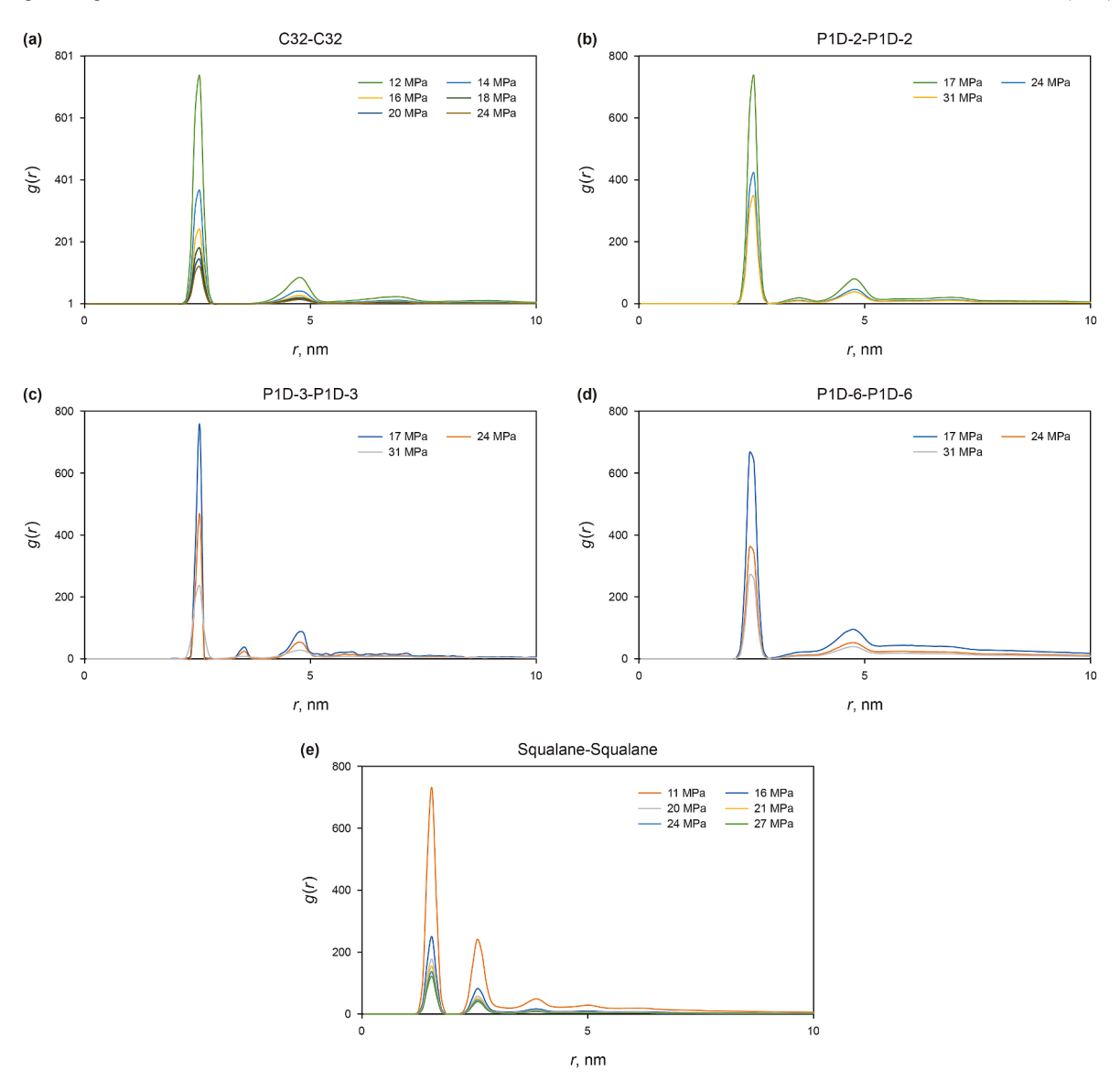


Fig. 8. The RDFs of (a) n-C32, (b) P1D-2, (c) P1D-3, (d) P1D-6 and (e) squalane under various pressures and 308 K.

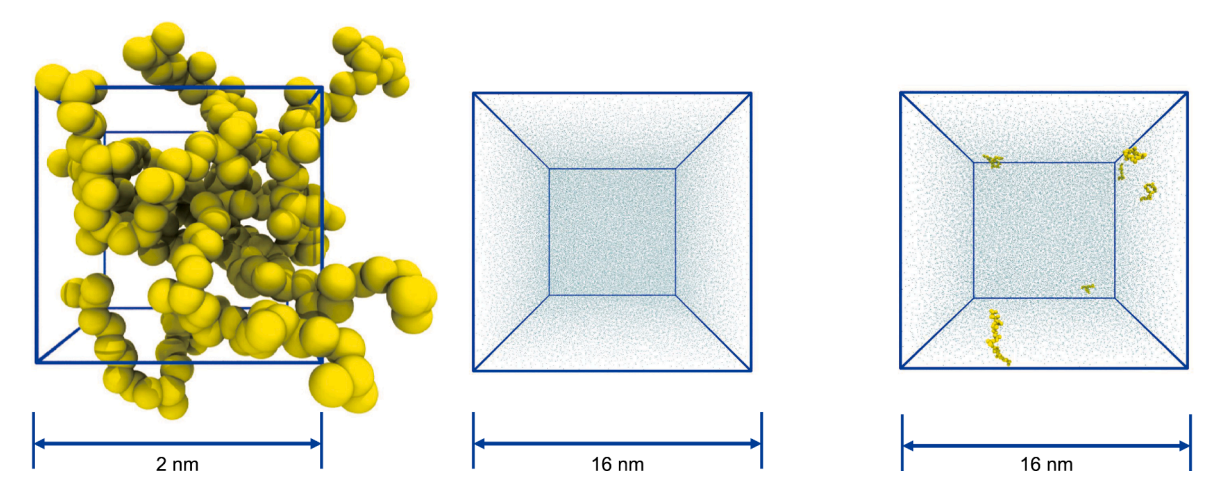


Fig. 9. Three kinds of systems. **(a)** The hydrocarbon oligomer systems with eight molecules; **(b)** The CO₂ system with 50,000 CO₂ molecules; **(c)** The hydrocarbon oligomer-CO₂ systems with eight oligomer and 50,000 CO₂ molecules.

Table 1Interaction energies between different types of hydrocarbon oligomers and CO₂ at 308 K and 24 MPa (energy unit: kJ/mol).

Types	$E_{ m oligomer+CO_2}$	$E_{ m oligomer}$	E_{CO_2}	E _{inter}
CO ₂ + n-C32	-208,011	-881	-202,929	-4,200
$CO_2 + P1D-2$	-208,728	-426	-202,929	-5,372
$CO_2 + P1D-3$	-208,789	-548	-202,929	-5,311
$CO_2 + P1D-6$	-208,678	-709	-202,929	-5,039
CO_2 + squalane	-207,508	-478	-202,929	-6,100

and the methine group (C1) has the largest interaction distance at 3.35 Å. In an RDF graph, a shorter interaction distance generally indicates a greater attraction. Fig. 11 clearly demonstrates a stronger interaction between the methyl group and CO₂.

Generally, a stronger interaction means more CO₂ molecules are surrounding the methylated fragment. To further explore the strength of the interaction between different fragments of hydrocarbon oligomer molecules and CO₂ molecules, we conduct a detailed study on the number of interactions between different fragments and CO₂. Based on the RDFs, we select the endpoint of the first shell of CO₂ molecules surrounding different fragments in n-C32, squalane, P1D-2, P1D-3 and P1D-6. We count the number of CO₂ molecules interacting with different pieces within the selected spatial range in the hydrocarbon oligomer simulation systems. And then, we calculate the average number of CO₂ molecules surrounding each fragment type. The results are shown in the right column in Fig. 11.

The right column in Fig. 11 shows that the number of methyl-containing particles in hydrocarbon oligomers interacting with CO_2 is significantly greater than that of other particles in the oligomer molecules. For example, in the squalane molecule, methyl particles (C3) interact with an average of 11.48 CO_2 molecules within the selected space, which is significantly higher than that of methylene(C1) and methine(C2) particles. On average, 20% more CO_2 molecules interacted with particles containing methyl groups than with other parts of the hydrocarbon oligomers. Therefore, we can understand that compared to other parts, the number of interactions between methylated fragment and CO_2 molecules attracted is the greatest and the interaction strength is the highest.

4. Conclusions

This study investigates the solubility of five hydrocarbon oligomers (n-C32, P1D-2, P1D-3, P1D-6, and squalane) in $scCO_2$ using MD, elucidating the effect of molecular structure on their solubility.

- (1) We employ a coarse-grained molecular model and utilized the DCM method to calculate the solubility of hydrocarbon oligomers in scCO₂. We find that the number of methyl groups and solubility positively correlate when molecular weights are similar. For example, the molecular weights of n-C32, P1D-3, and squalane are similar, with the number of methyl groups in their molecules gradually increasing (2, 4, and 8 methyl groups, respectively). Their solubility in scCO₂ under the same conditions also increases accordingly (0.2, 1.7, and 3.7 wt%, respectively).
- (2) The simulation results indicate that the increase in molecular weight of hydrocarbon oligomers weakens their solubility in scCO₂. However, the solubilities of P1D-2, P1D-3, and P1D-6 do not differ significantly (1.8, 1.7, and 1.6 wt%, respectively). This is mainly because, as the number of P1D repeating units increases, the molecular weight rises, and at the same time, the number of methyl groups within the molecule also increases.
- (3) We study the distribution morphology of hydrocarbon oligomers in scCO₂. The RDF analysis indicates that the minimum interaction distance between n-C32, P1D-2, P1D-3, and P1D-6 molecules exceeds 2 nm, while for squalane, it is approximately 1.5 nm. This suggests that hydrocarbon oligomer molecules do not viscosify through entanglement but exist as single dispersion in scCO₂. Thus, the interaction between hydrocarbon oligomer molecules and CO₂ molecules is key to their solubility.
- (4) In further analysis, we calculate the interaction energies of the five hydrocarbon oligomers with CO₂ under the same conditions. Results indicate that squalane exhibits the strongest interaction with CO₂ (6,100 kJ/mol), followed by P1D-2 (5,372 kJ/mol), P1D-3 (5,311 kJ/mol), and P1D-6 (5,039 kJ/mol). n-C32 shows the weakest interaction (4,200 kJ/mol). This indicates that the number of methyl groups in hydrocarbon oligomers affects their interaction

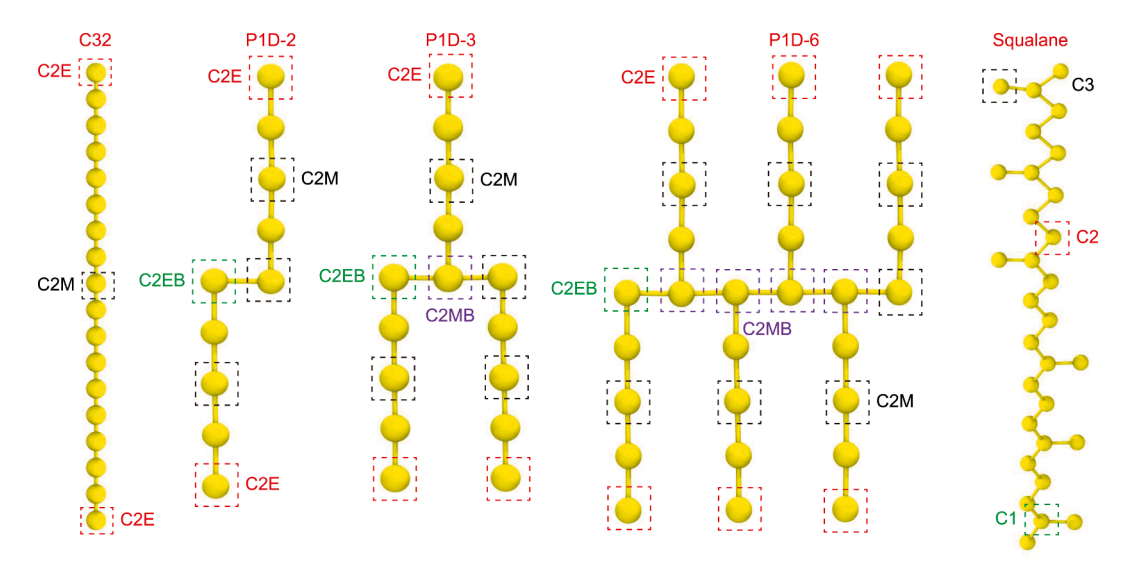


Fig. 10. The method for segmenting hydrocarbon oligomer molecules into distinct fragments.

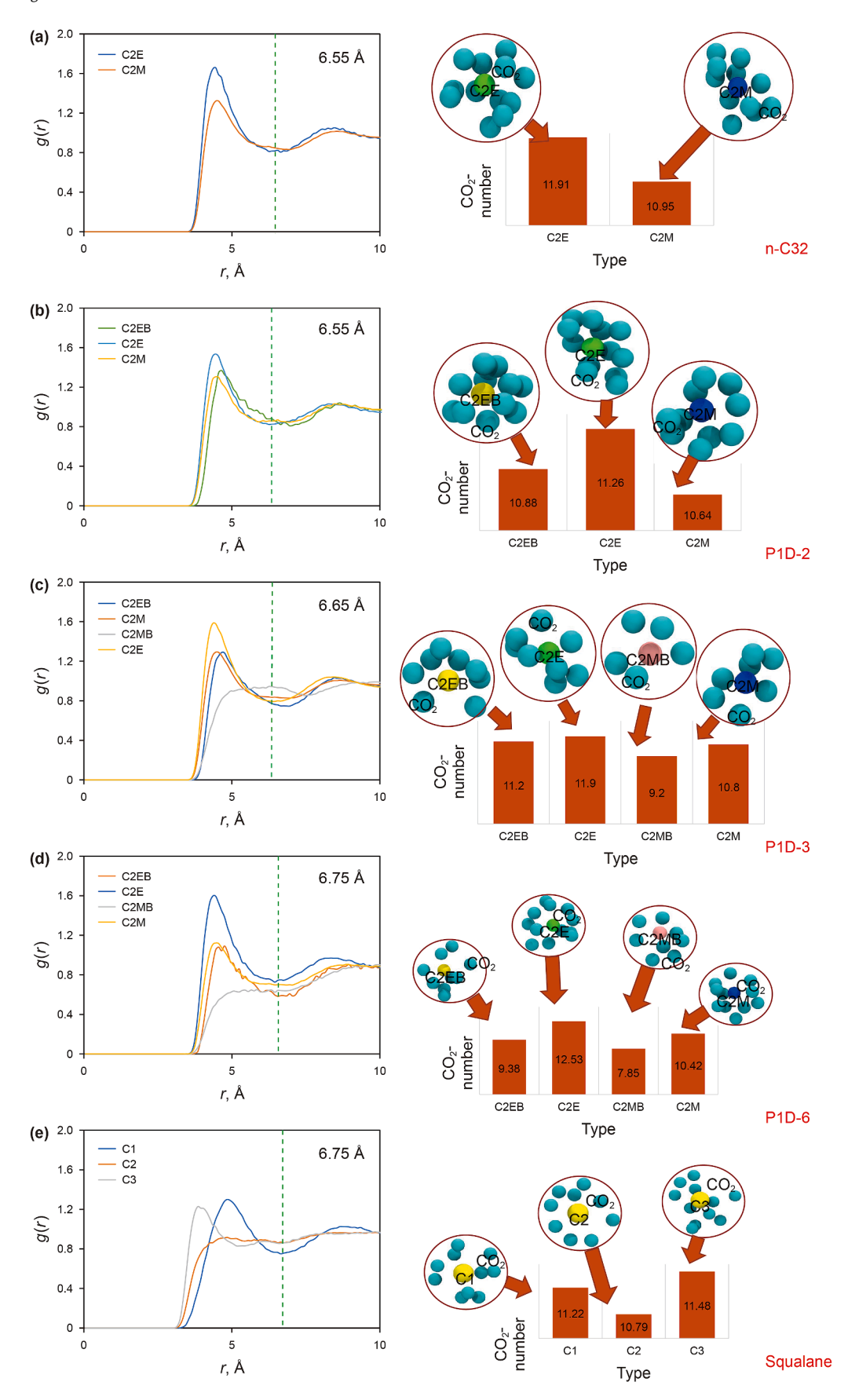


Fig. 11. Interaction between different hydrocarbon polymer fragments and CO₂ at 308 K and 24 MPa for different oligomers: (a) n-C32; (b) P1D-2; (c) P1D-3; (d) P1D-6 and (e) Squalane. The left column shows the RDF results while the right column describes the average number of CO₂ molecules surrounding each fragment type.

energy with CO₂, which is critical for determining their solubility.

- (5) To specifically illustrate the impact of methyl branches on solubility, we divide the hydrocarbon oligomer molecules into different segments and examined the interactions of various segments with CO₂. The RDF results show that the interaction distance between the methyl group and the CO₂ molecule is significantly smaller than that of other groups. For instance, in squalane, the interaction distance between the C3 (methyl) and the CO₂ molecule is 3.05 Å, which is much shorter than the distances for C2 (methylene) and C1 (methine), which are 3.15 Å and 3.35 Å, respectively.
- (6) Additionally, the number of interactions between CO₂ molecules and segments containing methyl groups is, on average, 20% higher than with other segments. This indicates that the presence of methyl groups significantly enhances the interactions between hydrocarbon oligomers and CO₂.

In summary, we explore the solubility differences of various hydrocarbon oligomers in scCO₂ and reveals the mechanism by which methyl groups influence their solubility. We also challenge the traditional theory that CO₂ viscosification polymers rely on molecular entanglement, emphasizing the dispersed state of hydrocarbon oligomers in scCO₂. Even though the squalane demonstrates better solubility compared to P1D-3, the viscosification is more effective for P1D-3. We attribute this to the synergistic effect between the methyl group and branching length. This work sets the stage for our ongoing molecular dynamics study in viscosification by hydrocarbon oligomers with different branching length and interfacial phenomenon of multiple systems.

CRediT authorship contribution statement

Ying Sun: Writing – original draft, Data curation, Formal analysis, Investigation, Methodology, Software. **Bin Wang:** Investigation, Writing – review & editing. **Haizhu Wang:** Funding acquisition, Investigation, Writing – review & editing. **Boxin Ding:** Writing – review & editing, Conceptualization, Formal analysis, Investigation, Project administration, Resources, Supervision, Validation, Funding acquisition.

Declaration of competing interest

The authors declare that they have no known competing financial interests or personal relationships that could have appeared to influence the work reported in this paper.

Acknowledgment

We sincerely acknowledge with thanks the financial support and funding provided by the National Natural Science Foundation of China (Youth Talent Program, Key Special Project, Grant No. 52341401 and Distinguished Scholar Program with a Grant No. 52425402), High-level Start-up Funding from Peking University Shenzhen Graduate School, Shenzhen Science and Technology Foundation (Grant No. JCYJ20230807120807016), High-level Start-up Funding from China University of Petroleum-Beijing (Grant No. 2462024YJRC033), the China Postdoctoral Science (CPS) Foundation (Certificate No. 2024M750106), and the Postdoctoral Fellowship Program of CPS (Grant No. GZC20240051). Boxin Ding is sincerely thankful for the insightful discussions with Professor Abbas Firoozabadi at Rice University.

References

- Afra, S., Alhosani, M., Firoozabadi, A., 2023. Improvement in CO₂ geo-sequestration in saline aquifers by viscosification: from molecular scale to core scale. Int. J. Greenh. Gas Control 125, 65–75. https://doi.org/10.1016/j.ijggc.2023.103888.
- Al-Abri, A., Sidiq, H., Amin, R., 2012. Mobility ratio, relative permeability and sweep efficiency of supercritical CO₂ and methane injection to enhance natural gas and condensate recovery: coreflooding experimentation. J. Nat. Gas Sci. Eng. 9, 166–171. https://doi.org/10.1016/j.jngse.2012.05.011.
- Al-Hinai, N., Saeedi, A., Wood, C., et al., 2018. Experimental evaluations of polymeric solubility and thickeners for supercritical CO₂ at high temperatures for enhanced oil recovery. Energy & Fuels 32, 1600–1611. https://doi.org/10.1021/acs.energyfuels.7b03733.
- An, Y., Bejagam, K., Deshmukh, S., 2018. Development of new transferable coarse-grained models of hydrocarbons. J. Phys. Chem. B. 122, 7143–7153. https://doi.org/10.1021/acs.jpcb.8b03822.
- Brehm, M., Kirchner, B., 2011. TRAVIS a free analyzer and visualizer for Monte Carlo and molecular dynamics trajectories. J. Chem. Inf. Model. 51, 2007–2023. https://doi.org/10.1021/ci200217w.
- Christensen, J., Stenby, E., Skauge, A., 2001. Review of WAG field experience. SPE Reservoir Eval. Eng. 4, 97–106. https://doi.org/10.2118/71203-Pa.
- Darden, T., York, D., Pedersen, L., 1993. Particle mesh Ewald: an Nlog (N) method for Ewald sums in large systems. J. Chem. Phys. 98, 10089–10092.
- Ding, B., Dong, M., Yu, L., 2020. A model of emulsion plugging ability in sandpacks: yield pressure drop and consistency parameter. Chem. Eng. Sci. 211. https://doi.org/10.1016/j.ces.2019.115248.
- Ding, B., Kantzas, A., Firoozabadi, A., 2024a. CO₂ trapping in layered porous media by effective viscosification. Water Resour. Res. 60, e2024WR037819.
- Ding, B., Kantzas, A., Firoozabadi, A., 2024b. Spatiotemporal X-Ray imaging of neat and viscosified CO₂ in displacement of brine-saturated porous media. SPE J. 29, 4426–4441. https://doi.org/10.2118/214842-pa.
- Ding, B., Sang, Q., Nie, Z., et al., 2021. An improved study of emulsion flooding for conformance control in a heterogeneous 2D model with lean zones. SPE J. 26, 3094–3108. https://doi.org/10.2118/206712-Pa.
- Espinosa, J., Young, J., Jiang, H., 2016. On the calculation of solubilities via direct coexistence simulations: investigation of NaCl aqueous solutions and Lennard-Jones binary mixtures. J. Chem. Phys. 145 (15), 154111. https://doi.org/10.1063/14964725.
- Feng, Y., Firoozabadi, A., 2023. Phase-field simulation of hydraulic fracturing by CO₂ and water with consideration of thermoporoelasticity. Rock Mech. Rock Eng. 56, 7333–7355. https://doi.org/10.1007/s00603-023-03355-7.
- Feng, Y., Haugen, K., Firoozabadi, A., 2021. Phase-field simulation of hydraulic fracturing by CO₂, water and nitrogen in 2D and comparison with laboratory data. J. Geophys. Res. Solid Earth 126 (11), e2021JB022509. https://doi.org/ 10.1029/2021jb022509
- Firoozabadi, A., Myint, P., 2010. Prospects for subsurface CO₂ sequestration. AIChE J. 56, 1398–1405. https://doi.org/10.1002/aic.12287.
- Gandomkar, A., Nasriani, H., Enick, R., et al., 2023. The effect of CO₂-philic thickeners on gravity drainage mechanism in gas invaded zone. Fuel 331 (1), 125760. https://doi.org/10.1016/j.fuel.2022.125760.
- Goicochea, A., Firoozabadi, A., 2019. Atomistic and mesoscopic simulations of the structure of CO₂ with fluorinated and nonfluorinated copolymers. J. Phys. Chem. C. 123, 17010–17018. https://doi.org/10.1021/acs.jpcc.9b04293.
- Heller, J., Dandge, D., Card, R., et al., 1985. Direct thickeners for mobility control of CO₂ floods. Soc. Petrol. Eng. J. 25, 679–686. https://doi.org/10.2118/11789-Pa.
- Higashi, H., Iwai, Y., Uchida, H., et al., 1998. Diffusion coefficients of aromatic compounds in supercritical carbon dioxide using molecular dynamics simulation. J. Supercrit. Fluids. 13, 93–97.
- Ho, J., Klamt, A., Coote, M., 2010. Comment on the correct use of continuum solvent models. J. Phys. Chem. 114, 13442–13444.
- Hoefling, T., Enick, R., Beckman, E., 1991. Microemulsions in near-critical and supercritical carbon dioxide. J. Phys. Chem. 95, 7127–7129.
- Hong, L., Tapriyal, D., Enick, R., 2008. Phase behavior of poly(propylene glycol) monobutyl ethers in dense CO₂. J. Chem. Eng. Data 53, 1342–1345. https://doi. org/10.1021/je800068v.
- Hoover, W., 1985. Canonical dynamics equilibrium phase-space distributions. Phys. Rev. 31, 1695–1697. https://doi.org/10.1103/PhysRevA.31.1695.
- Hou, L., Jiang, T., Liu, H., et al., 2017. An evaluation method of supercritical CO₂ thickening result for particle transporting. J. CO₂ Util. 21, 247–252. https://doi.org/10.1016/j.jcou.2017.07.023.
- Hu, D., Sun, S., Yuan, P., et al., 2015. Evaluation of CO₂-philicity of poly (vinyl acetate) and poly (vinyl acetate-alt-maleate) copolymers through molecular modeling and dissolution behavior measurement. J. Phys. Chem. B. 119, 3194–3204. https://doi.org/10.1021/jp5130052.
- Kar, T., Firoozabadi, A., 2022. Effective viscosification of supercritical carbon dioxide by oligomers of 1-decene. iScience 25 (5), 104266. https://doi.org/ 10.1016/j.isci.2022.104266.
- Kobayashi, K., Firoozabadi, A., 2023. Branching in molecular structure enhancement of solubility in CO₂. PNAS Nexus 2, 393. https://doi.org/10.1093/pnas-nexus/pgad393.
- Lemaire, P., Alenzi, A., Lee, J., et al., 2021. Thickening CO₂ with direct thickeners, CO₂-in-oil emulsions, or nanoparticle dispersions: literature review and experimental validation. Energy & Fuels 35, 8510–8540. https://doi.org/10.1021/acs.energyfuels.1c00314.

Li, N., Zhang, H., Ren, X., et al., 2024. Development status of supercritical carbon dioxide thickeners in oil and gas production: a review and prospects. Gas Sci. Eng. 125. https://doi.org/10.1016/j.jgsce.2024.205312.

- Li, Q., Wang, Y., Wang, Y., et al., 2018. Synthetic process on hydroxyl-containing polydimethylsiloxane as a thickener in CO₂ fracturing and thickening performance test. Energy Sources, Part A Recovery, Util. Environ. Eff. 40, 1137–1143. https://doi.org/10.1080/15567036.2018.1474297.
- Li, S., Zhang, D., 2019. How effective is carbon dioxide as an alternative fracturing fluid? SPE J. 24 (2), 857–876. https://doi.org/10.2118/194198-PA.
- Manzanilla-Granados, H., Saint-Martín, H., Fuentes-Azcatl, R., et al., 2015. Direct coexistence methods to determine the solubility of salts in water from numerical simulations. Test case NaCl. J. Phys. Chem. B 119, 8389–8396. https://doi.org/10.1021/acs.jpcb.5b00740.
- Martin, M., Siepmann, J., 1999. Novel configurational-bias Monte Carlo method for branched molecules. Transferable potentials for phase equilibria. 2. Unitedatom description of branched alkanes. J. Phys. Chem. B 103, 4508–4517. https://doi.org/10.1021/jp984742e.
- Middleton, R., Carey, J., Currier, R., et al., 2015. Shale gas and non-aqueous fracturing fluids: opportunities and challenges for supercritical CO₂. Appl. Energy 147, 500–509. https://doi.org/10.1016/j.apenergy.2015.03.023.
- Nose, S., 1984. A molecular-dynamics method for simulations in the canonical ensemble. Mol. Phys. 52, 255–268. https://doi.org/10.1080/00268978400101201.
- Parrinello, M., Rahman, A., 1981. Polymorphic transitions in single-crystals a new molecular-dynamics method. J. Appl. Phys. 52, 7182–7190. https://doi.org/ 10.1063/1.328693
- Riazi, M., Sohrabi, M., Jamiolahmady, M., 2011a. Experimental study of pore-scale mechanisms of carbonated water injection. Transport Porous Media 86, 73–86. https://doi.org/10.1007/s11242-010-9606-8.
- Riazi, M., Jamiolahmady, M., Sohrabi, M., 2011b. Theoretical investigation of porescale mechanisms of carbonated water injection. J. Petrol. Sci. Eng. 75, 312–326. https://doi.org/10.1016/j.petrol.2010.11.027.
- Ricky, E., Mwakipunda, G., Nyakilla, E., et al., 2023. A comprehensive review on CO₂ thickeners for CO₂ mobility control in enhanced oil recovery: recent advances and future outlook. J. Ind. Eng. Chem. 126, 69–91. https://doi.org/10.1016/j.jiec.2023.06.018.
- Rossen, W., Farajzadeh, R., Hirasaki, G., et al., 2022. Potential and challenges of foam-assisted CO₂ sequestration. SPE Improved Oil Recovery Conference. SPE,

D021S014R001.

- Schmid, N., Eichenberger, A., Choutko, A., et al., 2011. Definition and testing of the GROMOS force-field versions 54A7 and 54B7. European Biophysics Journal with Biophysics Letters 40, 843–856. https://doi.org/10.1007/s00249-011-
- Senapati, S., Keiper, J., DeSimone, J., et al., 2002. Structure of phosphate fluorosurfactant based reverse micelles in supercritical carbon dioxide. Langmuir 18, 7371–7376. https://doi.org/10.1021/la025952s.
- Shah, P., Cole, M., Beckman, E., et al., 2024. Advances in thickeners of CO₂: application potential of poly-1-decene. Gas Sci. Eng. 121, 205168. https://doi.org/10.1016/j.jgsce.2023.205168.
- Shen, Z., McHugh, M., Xu, J., et al., 2003. CO₂-solubility of oligomers and polymers that contain the carbonyl group. Polymer 44, 1491–1498. https://doi.org/10. 1016/S0032-3861(03)00020-X.
- Shokrollahi, A., Arabloo, M., Gharagheizi, F., et al., 2013. Intelligent model for prediction of CO₂-Reservoir oil minimum miscibility pressure. Fuel 112, 375–384. https://doi.org/10.1016/j.fuel.2013.04.036.
 Song, X., Guo, Y., Zhang, J., et al., 2019. Fracturing with carbon dioxide: from
- Song, X., Guo, Y., Zhang, J., et al., 2019. Fracturing with carbon dioxide: from microscopic mechanism to reservoir application. Joule 3, 1913–1926. https:// doi.org/10.1016/j.joule.2019.05.004.
- Sun, B., Sun, W., Wang, H., et al., 2018. Molecular simulation aided design of copolymer thickeners for supercritical CO₂ as non-aqueous fracturing fluid. J. CO₂ Util. 28, 107–116. https://doi.org/10.1016/j.jcou.2018.09.015.
- Sun, Y., Zhang, D., Bashir, A., et al., 2023. Scaling Solute-solvent distances to improve solubility and ion paring predictions in rigid ion models. J. Phys. Chem. B 127 (44), 9575–9586. https://doi.org/10.1021/acs.jpcb.3c05993.
- Takuma, K., Maeda, Y., Watanabe, Y., et al., 2024. CO₂ fracturing of volcanic rocks under geothermal conditions: characteristics and process. Geothermics 120, 103007. https://doi.org/10.1016/j.geothermics.2024.103007.
- Van der Spoel, D., Lindahl, E., Hess, B., et al., 2005. GROMACS: fast, flexible, and free. J. Comput. Chem. 26, 1701–1718. https://doi.org/10.1002/jcc.20291.
- Zaberi, H., Lee, J., Enick, R., et al., 2020. An experimental feasibility study on the use of CO₂-soluble polyfluoroacrylates for CO₂ mobility and conformance control applications. J. Petrol. Sci. Eng. 184, 106556. https://doi.org/10.1016/j. petrol.2019.106556.
- Zhang, S., She, Y., Gu, Y., 2011. Evaluation of polymers as direct thickeners for CO₂ enhanced oil recovery. J. Chem. Eng. Data 56, 1069–1079. https://doi.org/10.1021/ie1010449.